http://dx.doi.org/10.5012/bkcs.2013.34.9.2769

Pycnometric and Spectroscopic Studies of Red Phosphors $Ca^{2+}_{(1-1.5x)}WO_4:Eu^{3+}_x$ and $Ca^{2+}_{(1-2x)}WO_4:Eu^{3+}_x,Na^{+}_x$

Seon-Woog Cho

Department of Materials Science and Engineering, Silla University, Busan 617-736, Korea. E-mail: swcho@silla.ac.kr
Received May 20, 2013, Accepted June 27, 2013

Red phosphors $Ca_{(1-1.5x)}Eu_xWO_4$ and $Ca_{(1-2x)}Eu_xNa_xWO_4$ were synthesized with various concentrations x of Eu^{3+} ions by using a solid-state reaction method. The crystal structure of the red phosphors were found to be a tetragonal scheelite structure with space group $I4_1/a$. X-ray diffraction (XRD) results show the (112) main diffraction peak centered at $2\theta = 28.71^o$, and indicate that there is no basic structural deformation caused by the vacancies V_{Ca}'' or the Eu^{3+} (and Na^+) ions in the host crystals. Densities of $Ca_{(1-1.5x)}Eu_xWO_4$ were measured on a (helium) gas pycnometer. Comparative results between the experimental and theoretical densities reveal that Eu^{3+} (and Na^+) ions replace the Ca^{2+} ions in the host $CaWO_4$. Also, the photoluminescence (PL) emission and photoluminescence excitation (PLE) spectra show the optical properties of trivalent Eu^{3+} ions, not of divalent Eu^{2+}. Raman spectra exhibit that, without showing any difference before and after the doping of activators to the host material $CaWO_4$, all the gerade normal modes occur at the identical frequencies with the same shapes and weaker intensities after the substitution. However, the FT-IR spectra show that some of the ungerade normal modes have shifted positions and different shapes, caused by different masses of Eu^{3+} ions (or Na^+ ions, or V_{Ca}'' vacancies) from Ca^{2+}.

Key Words : Scheelite, $Ca_{(1-1.5x)}Eu^{3+}_x WO_4$, $Ca_{(1-2x)}Eu^{3+}_x Na^{+}_x WO_4$, Gas pycnometer, Raman and FT-IR

Introduction

In a previous paper,[1] we presented the synthesis and photoluminescence properties of $CaWO_4:Eu^{3+}$ phosphors. The host material $CaWO_4$ exhibits a bright blue fluorescence upon exposure to a short wavelength ultraviolet radiation (254 nm). $CaWO_4$ crystallizes in the tetragonal scheelite structure (space group: $I4_1/a$),[2-6] at ambient temperature and pressure. Calcium tungstate $Ca^{2+}WO_4^{2-}$ is essentially an ionic compound. The Ca^{2+} ions are 8-fold coordinated to oxide ions from eight separate WO_4^{2-} tetrahedra. Europium can substitute for Ca^{2+} in scheelite as either Eu^{3+} or Eu^{2+}.[7] The substitution of trivalent for divalent requires a charge compensating mechanism to maintain electrical neutrality. If it enters as trivalent , it enters scheelite by either the vacancy V_{Ca}'' or Na^+ coupled substitution mechanism:[8]

$$3Ca_{Ca}^{\times} = 2Eu_{Ca}^{\cdot} + V_{Ca}'' \quad (1)$$

and

$$2Ca_{Ca}^{\times} = Eu_{Ca}^{\cdot} + Na_{Ca}' \quad (2)$$

in Kröger-Vink notation.[9] Mechanism (1) creates one vacancy for every substitution of two Eu^{3+} ions into three Ca^{2+} sites. However, mechanism (2) does not make any vacancy. The vacancies may have bigger or smaller volume than the ion which is removed. The removal of a cation causes the effect of the nearest neighbor anions to experience a charge repulsion among anions, which are unshielded by the cation. The vacancies shall have its own space with some size. These point defects must be revealed as a change of density on the addition of Eu^{3+} to $CaWO_4$.

The effective ionic radius of Eu^{3+} in 8-fold coordination is 106.6 pm.[10,11] If Eu^{2+} substitute for Ca^{2+}, its ionic radius size (125 pm) in 8-fold coordination is much greater than the size of Ca^{2+} (112 pm). Because of the larger ionic size, the possibility of substitution of Eu^{2+} into the host $CaWO_4$ is very low, though not impossible, compared with that of Eu^{3+}. We have observed only features of Eu^{3+} from the PLE and PL results of Paper 1 (Ref. 1), not of Eu^{2+}. To show a more direct evidence for the formation of vacancies in accordance with mechanism (1), here we report pycnometric measurements of $Ca_{(1-1.5x)}Eu_xWO_4$ powder samples as a function of europium concentration x. Physical characterization of newly synthesized $Ca_{(1-2x)}Eu_xNa_xWO_4$ are also reported. Also presented are the Raman and FT-IR studies of the red phosphors.

Experimental

Using a solid-state reaction method, as in the Paper 1, $Ca_{(1-1.5x)}Eu_xWO_4$ and $Ca_{(1-2x)}Eu_xNa_xWO_4$ were synthesized with various concentrations x of Eu^{3+} ions. The concentrations of europium were x = 0, 0.02, 0.04, 0.06, 0.08, 0.10, and 0.12. All the starting materials were purchased from Sigma-Aldrich Korea. After mixing and grinding on an agate mortar, the reactants were put into an electric tube furnace. Heating and cooling rates were less than 4 °C/min. Following calcination, the highest sintering temperature reached up to 1,100 °C for $Ca_{(1-1.5x)}Eu_xWO_4$. This sintering temperature was lowered to 950 °C for $Ca_{(1-2x)}Eu_xNa_xWO_4$, because they form partly fused clusters of powder on a high

temperature. The chemical reactions are

$$(1-1.5x)CaCO_3 + WO_3 + (x/2)Eu_2O_3 \rightarrow Ca_{(1-1.5x)}Eu_xWO_4 + (1-1.5x)CO_2 \quad (3)$$

and

$$(1-2x)CaCO_3 + WO_3 + (x/2)Eu_2O_3 + (x/2)Na_2CO_3 \rightarrow Ca_{(1-2x)}Eu_xNa_xWO_4 + (1-1.5x)CO_2 \quad (4)$$

and the ceramic phosphors were produced in a powder form. Crystal structure is determined by a X-ray diffractometer, Philips PANalytical X'Pert. The optical properties are obtained from photoluminescence (PL) emission and photoluminescence excitation (PLE) on a fluorescence spectrometer, Scinco FS-2.

Gas pycnometer AccuPyc II 1340 was used to determine the density of the ceramic powder samples. Gas pycnometer is an analytical technique that use a gas displacement method to measure volume accurately. Here, helium is used as the displacement medium. The operations were done in room temperature (average 22.3 ºC). Every sample was measured the density for three times and obtained the average and standard deviation. In addition, micro-Raman and Fourier transform infrared (FT-IR) spectroscopies were performed on a microscopic FT-IR/Raman (Vertex 80V, Bruker).

Results and Discussion

Figure 1 shows photoluminescence excitation (PLE) and photoluminescence emission (PL) spectra of $Ca_{(1-1.5x)}Eu_xWO_4$ and $Ca_{(1-2x)}Eu_xNa_xWO_4$ phosphors synthesized with various europium concentrations. Here we present only the results of three samples prepared, because the rest exhibits the same characteristic features except with weaker intensities depending on the concentration x of Eu, showing the same peak shapes. The excitation spectra of these systems (λ_{em} = 615 nm) consist of a broad band and some sharp lines: (1) The broad band 220-340 nm is attributed to $O^{2-} \rightarrow W^{6+}$ charge transfer band (CTB) centered 261 nm and $O^{2-} \rightarrow$

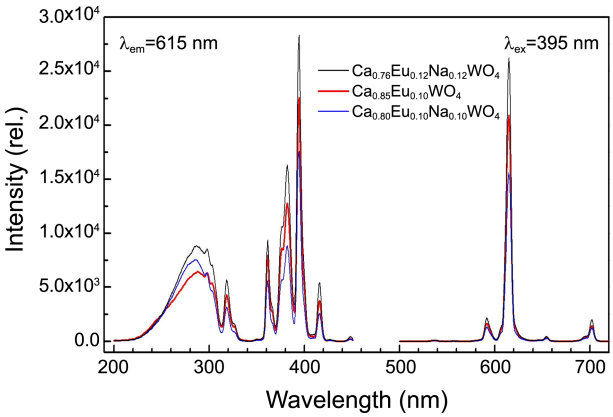

Figure 1. Photoluminescence excitation (PLE) and photoluminescence emission (PL) spectra of $Ca_{0.85}Eu_{0.10}WO_4$, $Ca_{0.80}Eu_{0.10}Na_{0.10}WO_4$ and $Ca_{0.76}Eu_{0.12}Na_{0.12}WO_4$ phosphors.

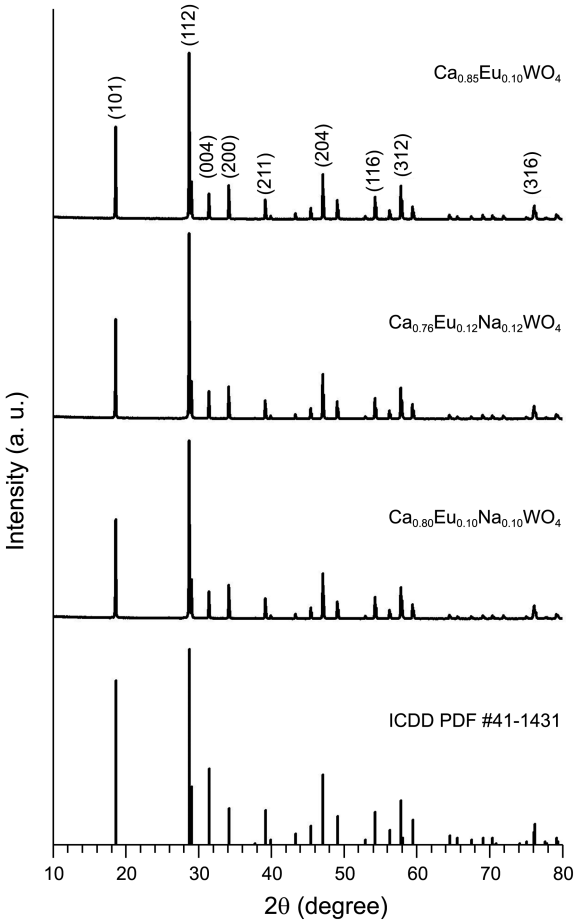

Figure 2. Powder XRD patterns of $Ca_{0.85}Eu_{0.10}WO_4$, $Ca_{0.80}Eu_{0.10}Na_{0.10}WO_4$ and $Ca_{0.76}Eu_{0.12}Na_{0.12}WO_4$ phosphors.

Eu^{3+} CTB around 280 nm, overlapped with the narrow ${}^7F_0 \rightarrow {}^5F_{2,4}$ and ${}^7F_0 \rightarrow {}^5H_3$ transitions from the Eu^{3+} ion.[1,12,13] (2) In the range 340-450 nm, the intraconfigurational 4f-4f transitions are observed. Peaks at 362, 382, 395, and are assigned as the transitions from the ground state ${}^7F_0$ to ${}^5D_4$, ${}^5L_7$, ${}^5L_6$, and ${}^5D_3$, respectively.[1,12,13] Only notable difference in PLE between $Ca_{(1-1.5x)}Eu_xWO_4$ and $Ca_{(1-2x)}Eu_xNa_xWO_4$ is a somewhat stronger $O^{2-} \rightarrow Eu^{3+}$ CTB centered around 280 nm for $Ca_{(1-2x)}Eu_xNa_xWO_4$. In PL emission 500-720 nm (with λ_{ex} = 395 nm) we find no characteristic difference between $Ca_{(1-1.5x)}Eu_xWO_4$ and $Ca_{(1-2x)}Eu_xNa_xWO_4$. The sharp lines at 594, 615, 648, and 700 nm correspond to ${}^5D_0 \rightarrow {}^7F_J$ (J = 1, 2, 3, 4) transitions, respectively.[1,14,15] It has been found that[16] the phosphors with efficient charge compensation, both $Ca_{(1-1.5x)}Eu_xWO_4$ and $Ca_{(1-2x)}Eu_xNa_xWO_4$, show enhanced luminescence of Eu^{3+} more than 3 times compared with that of a commercial red phosphor $Y_2O_2S:Eu^{3+}$. Here in this work one of the main differences between $Ca_{(1-1.5x)}Eu_xWO_4$ and $Ca_{(1-2x)}Eu_xNa_xWO_4$ is the x value, which is showing the concentration quenching. The vacancy included formula $Ca_{(1-1.5x)}Eu_xWO_4$ exhibit the concentration quenching at around x = 0.10.[1] However, the Na co-doped $Ca_{(1-2x)}Eu_xNa_xWO_4$ show concentration quenching at over x = 0.12 with a stronger intensity. So the intensity *versus* x of $Ca_{(1-2x)}Eu_xNa_xWO_4$ shows rather slow

increase at an earlier stage but much stronger intensity at a later stage of x.

Figure 2 shows XRD spectra of $Ca_{(1-1.5x)}Eu_xWO_4$ and $Ca_{(1-2x)}Eu_xNa_xWO_4$ ceramic powders. The XRD patterns of the prepared phosphors correspond to the International Centre for Diffraction Data (ICDD) Powder Diffraction File (PDF) 41-1431, without showing any significant difference on the concentration of Eu. Diffraction angles 2θ for the planes (101), (112), (004), (200), (211), (204), (116), (312), and (316) are 18.60°, 28.71°, 31.42°, 34.14°, 39.17°, 47.08°, 54.29°, 57.84°, and 76.17°, respectively. It belongs to the body-centered tetragonal system and space group $I4_1/a$, with cell constants a = 5.243 Å and c = 11.373 Å. There are four $CaWO_4$ molecules per unit cell; Z = 4.[2] In accordance with the results of Shi *et al.*[16] we found little difference for the d-spacing values of (112) planes due to the distinct ionic radii among Ca^{2+} (112 pm), Eu^{3+} (106.6 pm), and Na^+ (118 pm). The largest difference is shown for x = 0.12 of $Ca_{(1-1.5x)}Eu_xWO_4$, with $\Delta 2\theta = (28.71-28.69)^\circ = 0.02^\circ$. We are not surprised in the case of co-doped $Ca_{(1-2x)}Eu_xNa_xWO_4$, because the sum of two calcium ions perfectly matches, coincidentally, with the sum of europium and sodium ions in matter of size. So we used cell volume V_c = 312.63 Å^3, for the sake of brevity, later for the calculation of density, even though the cell volume must show small shrinkage following Vegard's law[17] with increasing x values.

Bird's eye view, or c axis projection, of the $CaWO_4$ unit cell crystal structure is shown in Figure 3, which is adopted from Ref. 6 and redrawn. Five *ab*-planes are presented along c axis, from the top to the bottom. WO_4^{2-} tetrahedra are flattened in the c direction, with $\bar{4}$ (or S_4 in Schönflies notation) symmetry. Ca^{2+} also has site symmetry $\bar{4}$. The calcium ions are 8-fold coordinated with the oxygen atoms of four surrounding tungstate groups. Sixteen oxygen atoms in the unit cell are on site symmetry 1 (or C_1).

The most direct evidence for the formation of vacancies or point defects is obtained by determining the lattice constant (from XRD) for a structure in order to compare theoretical with measured crystal density (from pycnometer). Figure 4 shows a comparison of change in density on the addition of europium to $CaWO_4$. Actual crystal densities are determined by pycnometric measurements of $Ca_{(1-1.5x)}Eu_xWO_4$ powder samples. Theoretical vacancy model calculations are based on the lattice parameter measured using X-ray diffraction, cell volume V_c = 312.63 Å^3. For example, a crystal with the composition $Ca_{0.85}Eu_{0.10}WO_4$ has density as the following: there are $4 \times 0.85 \times 40.078/(6.022 \times 10^{23})$ g Ca, $4 \times 0.10 \times 151.964/(6.022 \times 10^{23})$ g Eu, $4 \times 1 \times 183.84/(6.022 \times 10^{23})$ g W, and $4 \times 4 \times 15.9994/(6.022 \times 10^{23})$ g O in 312.63 Å^3 for a calculated density of 6.3123 g/cm^3. If europium enters into $CaWO_4$ as Eu^{2+} with no vacancy, it will be $Ca_{0.90}Eu_{0.10}WO_4$ and the calculated density should be 6.3549 g/cm^3. The experimental result for x = 0.10 is 6.2378 g/cm^3, which is much closer to that of $Ca_{(1-1.5x)}Eu_xWO_4$. However the numbers are not perfectly matching yet, partly because we measured the volume of powder samples. Powder is a solid state of fine loose particles consisted of different shapes and sizes. If we could grow a crystal of $Ca_{(1-1.5x)}Eu_xWO_4$, instead of powder, and measured the volume, it would yield more accurate agreement. However we see that, in Figure 4, the

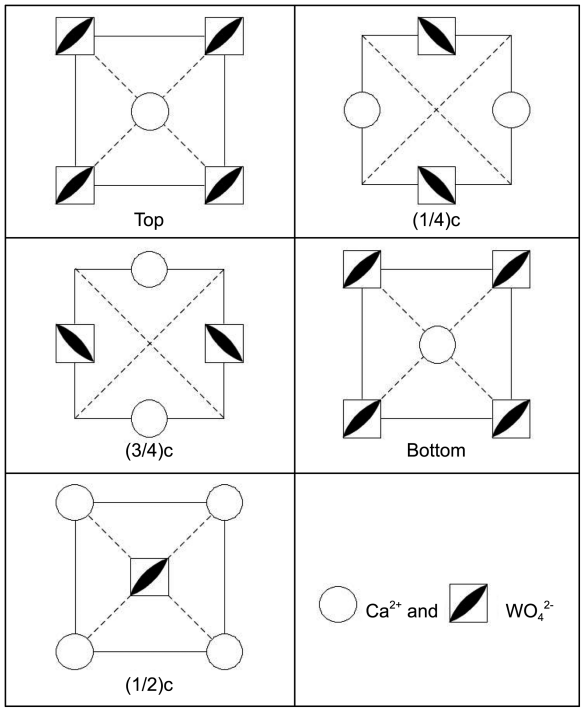

Figure 3. Bird's eye view, or c axis projection, of the $CaWO_4$ unit cell crystal structure. There are four $CaWO_4$ molecules in the unit cell. Along c axis, from the top to the bottom, five *ab*-planes are presented. WO_4^{2-} tetrahedra are flattened in the c direction, with $\bar{4}$ symmetry. Site symmetry of Ca^{2+} is also $\bar{4}$.

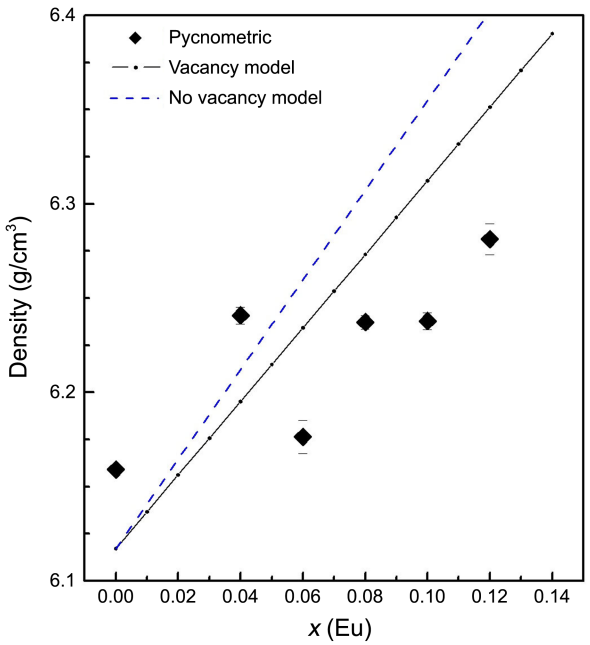

Figure 4. A comparison of change in density on the addition of europium to $CaWO_4$. Actual crystal densities are determined by pycnometric measurements of $Ca_{(1-1.5x)}Eu_xWO_4$ powder samples. Theoretical vacancy model calculations are based on the lattice parameter measured using a X-ray diffraction.

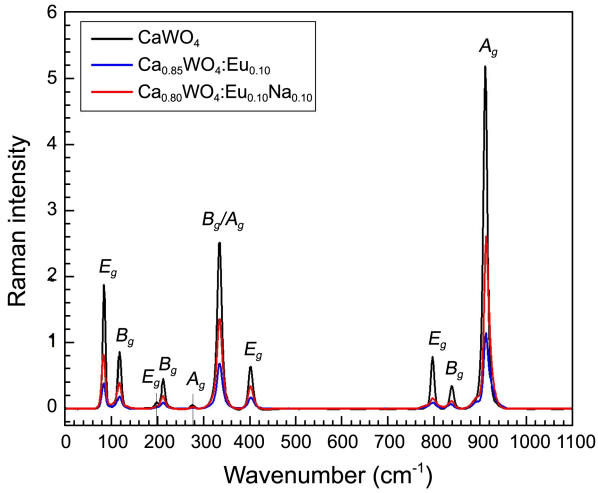

Figure 5. FT-Raman spectra of $CaWO_4$, $Ca_{0.85}Eu_{0.10}WO_4$, and $Ca_{0.80}Eu_{0.10}Na_{0.10}WO_4$.

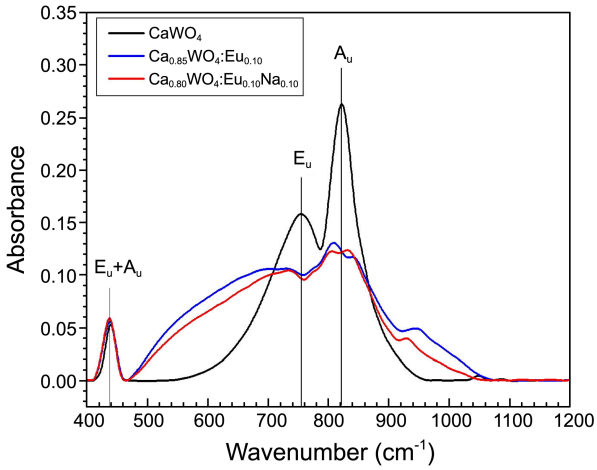

Figure 6. FT-IR spectra of $CaWO_4$, $Ca_{0.85}Eu_{0.10}WO_4$, and $Ca_{0.80}Eu_{0.10}Na_{0.10}WO_4$.

pycnometrically determined results basically follow the line of vacancy model. This result strongly suggest that two Eu^{3+} ions and one V_{Ca}'' vacancy replace three Ca^{2+} ions in the host $CaWO_4$, creating $Ca_{(1-1.5x)}Eu_xWO_4$. If the lattice does not shrink around a missing calcium ion, we can estimate the size of vacancy that replaces the Ca site from the difference between the radii of Ca^{2+} and Eu^{3+} as follows: $3r_{Ca^{2+}} = 2r_{Eu^{3+}} + r_{V_{Ca}}$. Using ionic radii from Shannon[10,11] for 8-fold coordination we obtain the radius of vacancy: $r_{V_{Ca}} = 3r_{Ca^{2+}} - 2r_{Eu^{3+}} = 3(112\text{ pm}) - 2(106.6\text{ pm}) = 122.8\text{ pm}$.

Raman scattering and FT-IR spectroscopy are experimental techniques that provide informations about the vibrational properties of materials. Figure 5 shows the FT-Raman spectra of $CaWO_4$, $Ca_{(1-1.5x)}Eu_xWO_4$, and $Ca_{(1-2x)}Eu_xNa_xWO_4$. And Figure 6 presents the FT-IR spectra of $CaWO_4$, $Ca_{(1-1.5x)}Eu_xWO_4$, and $Ca_{(1-2x)}Eu_xNa_xWO_4$. The $CaWO_4$ crystals have 26 distinct vibrational modes:[18-20]

$$\Gamma = 3A_g + 5A_u + 5B_g + 3B_u + 5E_g + 5E_u \quad (5)$$

where the subscript g (gerade) and u (ungerade) indicate the parity under inversion. Among these, 13 Raman active modes are expected:

$$\Gamma_{Raman} = 3A_g + 5B_g + 5E_g \quad (6)$$

and only 8 IR active vibrational modes:

$$\Gamma_{IR} = 4A_u + 4E_u \quad (7)$$

The results of Raman spectra in Figure 5 reveal that all the gerade mode has the same frequencies before and after the replacement of Ca^{2+} with Eu^{3+} (or Na^+ ion, or V_{Ca}'' vacancy), except somewhat weaker intensity of each peak after the substitution. This trend is more apparent for $Ca_{(1-1.5x)}Eu_xWO_4$, which has vacancies in the structure. The positions and shapes of each peak are almost identical with those of Gracia *et al.*[19] and Cavalcante *et al.*[20] In Figure 5, the positions of E_g, B_g, B_g, B_g/A_g, E_g, E_g, B_g, and A_g are as follows: 84, 117, 212, 334, 401, 797, 839, and 912 cm^{-1}, respectively.

A notable feature of scheelite structure is the existence of $[WO_4]$ and $[CaO_8]$ clusters as isolated tetrahedra and snub bisdisphenoid (12-faced) polyhedra, individually, in the crystal structure. Point group of snub bisdisphenoid is D_{2d}. Calcium and tungsten atoms are never bonded directly, so the bonding sequence throughout the crystal is –O–W–O–Ca–O–W–. IR results in Figure 6 reveal that ungerade vibrations are very different after the replacement of Ca^{2+}. The positions of E_u+A_u, E_u, and A_u modes in $CaWO_4$ are 439, 754, and 822 cm^{-1}, respectively. These numbers show close agreement with reported experimental data.[20,21] The E_u+A_u vibrations at 439 cm^{-1} do not show any noticeable change after doping. However, E_u and A_u vibrations of 754 and 722 cm^{-1} drastically change following the substitution. Both peaks now become swollen bands covering wide range of frequencies. Our conclusion from Figure 6 is that the clusters $[EuO_8]$, $[NaO_8]$, and $[V_{Ca}O_8]$ created within after the substitution of Ca^{2+} with Eu^{3+}, etc. break symmetry of the host crystal $CaWO_4$ and appear as antisymmetric ungerade vibrations in $Ca_{(1-1.5x)}Eu_xWO_4$ and $Ca_{(1-2x)}Eu_xNa_xWO_4$. This local distortion caused by point defect is more severe in $Ca_{(1-1.5x)}Eu_xWO_4$, in which vacancies came into inherently, than in $Ca_{(1-2x)}Eu_xNa_xWO_4$.

Conclusion

By using a solid-state reaction method two kinds of ceramic phosphors $Ca_{(1-1.5x)}Eu_xWO_4$ and $Ca_{(1-2x)}Eu_xNa_xWO_4$ were synthesized with different concentrations x of Eu^{3+} ions. The PL and PLE spectra show the optical properties of trivalent ion Eu^{3+}, not of divalent Eu^{2+}. Densities of $Ca_{(1-1.5x)}Eu_xWO_4$ were measured on a helium gas pycnometer. Comparison between the experimental and calculated model densities show that trivalent Eu^{3+} ions replace the Ca^{2+} ions in the host $CaWO_4$, and create vacancies in $Ca_{(1-1.5x)}Eu_xWO_4$. XRD results show that there is no basic structural deformation caused by the vacancies V_{Ca}'' or the Eu^{3+} (and Na^+) ions in the host crystals. The crystal structure of the red phosphors were found to be a tetragonal scheelite structure with space group $I4_1/a$. Raman spectra reveal that,

without showing any difference before and after the doping of activators to the host material $CaWO_4$, all the gerade normal modes occur at the identical frequencies with the same shapes and weaker intensities after the substitution. The phenomena of weaker intensities are more apparent in $Ca_{(1-1.5x)}Eu_xWO_4$, in which $0.5x$ vacancies inherently exist, than $Ca_{(1-2x)}Eu_xNa_xWO_4$. The FT-IR spectra show that some of the ungerade normal modes have shifted positions and different shapes, caused by different masses of Eu^{3+} ions (or Na^+ ions, or V_{Ca}'' vacancies) from Ca^{2+}. The clusters $[EuO_8]$, $[NaO_8]$, and $[V_{Ca}O_8]$ created within after the substitution of Ca^{2+} with Eu^{3+}, etc. cause the effects of symmetry breaking of the host crystal $CaWO_4$ and appear as antisymmetric ungerade vibrations in $Ca_{(1-1.5x)}Eu_xWO_4$ and $Ca_{(1-2x)}Eu_xNa_xWO_4$. In conclusion, point defects, especially vacancies, are disclosed successfully through pycnometrical and spectroscopic determinations.

Acknowledgments. The density determination was done on a Micrometrics AccuPyc II 1340, provided by Protech Korea. XRD and FT-IR/Raman spectra were obtained using the facilities of Korea Basic Science Institute (KBSI). The author is grateful to Protech Korea and KBSI.

References

1. Cho, S.; Cho, S.-W. *Kor. J. Mater. Res.* **2012**, *22*, 215.
2. Blanchard, F. *Powder Diffraction* **1989**, *4*, 220.
3. Zalkin A.; Templeton, D. H. *J. Chem. Phys.* **1964**, *40*, 501.
4. Kay, M. I.; Frazer, B. C.; Almodovar, I. *J. Chem. Phys.* **1964**, *40*, 504.
5. Sleight, A. W. *Acta Cryst.* **1972**, *B28*, 2899.
6. Warner, T. E. *Synthesis, Properties and Mineralogy of Important Inorganic Materials*; John Wiley and Sons: U. K., 2011; pp 228-239.
7. McCarthy, G. J. *Mat. Res. Bull.* **1971**, *6*, 31.
8. Ghaderi, M.; Palin, J. M.; Campbell, I. H.; Sylvester, P. J. *Economic Geology* **1999**, *94*, 423.
9. Connelly, N. G.; Damhus, T.; Hartshorn, R. M.; Hutton, A. T. *Nomenclature of Inorganic Chemistry, IUPAC Recommendations 2005*; RSC Publishing: Cambridge, U. K., 2005.
10. Shannon, R. D. *Acta Cryst.* **1976**, *A32*, 751.
11. Shannon, R. D.; Prewitt, C. T. *Acta Cryst*. **1969**, *B25*, 925.
12. Kodaira, C. A.; Brito, H. F.; Felinto, M. C. F. C. *Journal of Solid State Chemistry* **2003**, *171*, 401.
13. Kodaira, C. A.; Brito, H. F.; Malta, O. L.; Serra, O. A. *Journal of Luminescence* **2003**, *101*, 11.
14. Huang, J.; Xu, J.; Luo, H.; Yu, X.; Li, Y. *Inorg. Chem.* **2011**, *50*, 11487.
15. Su, Y.; Li, L.; Li, G. *Chem. Mater.* **2008**, *20*, 6060.
16. Shi, S.; Gao, J.; Zhou, J. *Optical Materials* **2008**, *30*, 1616.
17. Cullity, B. D.; Stock, S. R. *Elements of X-Ray Diffraction*, 3rd ed.; Prentice Hall, U. S. A., 2001; p 339.
18. Rousseau, D. L.; Bauman, R. P.; Porto, S. P. S. *J. Raman Spectrosc.* **1981**, *10*, 253.
19. Gracia, L.; Longo, V. M.; Cavalcante, L. S.; Beltran, A.; Avansi, W.; Li, M. S.; Mastelaro, V. R.; Varela, J. A.; Longo, E.; Andrs, J. *J. Appl. Phys*. **2011**, *110*, 043501.
20. Cavalcante, L. S.; Longo, V. M.; Sczancoski, J. C.; Almeida, M. A.; Batista, J. A.; Varela, J. A.; Orlandi, M. O.; Longo, E.; Li, M. S. *CrystEngComm* **2012**, *14*, 853.
21. Burcham, L. J.; Wachs, I. E. *Spectrochimica Acta Part A* **1998**, *54*, 1355.